Asociación Argentina
de Mecánica Computacional

Mecánica Computacional Vol XXVI, pp.3644-3663
Sergio A. Elaskar, Elvio A. Pilotta, Germán A. Torres (Eds.)
Córdoba, Argentina, Octubre 2007

.

VELOCITY AND TEMPERATURE NATURAL DISSIMILARITY IN A TURBULENT CHANNEL FLOW

Hugo D. Pasinato

Din. Fluidos y Fen. Transporte Computacinal, Departamento de Ingeniería Química,
UAC, Universidad Tecnológica Nacional,
Plaza Huincul, Neuquén, hpasinato@uacf.utn.edu.ar,
http://www.uacf.utn.edu.ar

Keywords: Velocity and temperature dissimilarity, Scalar transport, Wall turbulent flow, Direct Numerical Simulation.

Abstract. Natural dissimilarity or de-correlation of axial velocity and temperature fluctuations, in a turbulent channel flow, is studied using direct numerical simulation, DNS. Buoyancy effects were neglected, thus the temperature was considered as a passive scalar. A uniform energy source case for the thermal field has been used. Results for molecular Pr or Sc numbers equal to 1.0 and 0.71 are presented. More evidences of the strong correlation of axial velocity and temperature in the wall layer are shown, like as the similar patter of the skin-friction and streamwise vorticity correlation, with that between wall heat flux and streamwise vorticity correlation. The importance of the most energetic events on the dissimilarity between the axial velocity and temperature fluctuations is examined using conditional probability. It is shown that although the most energetic events are responsible of the strongest instantaneous dissimilarities, their contribution to the mean dissimilarity is less than a half in the whole channel. As a complement to many previous results in the literature analyzing fluctuations of longitudinal velocity and temperature in frequency domain, spectral density functions is used in order to study dissimilarity. The results presented here include new variables, as the spectra of the fluctuations of axial velocity and temperature difference, and the spectra of the fluctuations of the pressure field. Spectral density functions at different distances from the wall show, that the main cause of dissimilarity between axial velocity and temperature fluctuations is the shift toward higher frequencies of temperature in comparison to any velocity components, and specially to axial velocity, in the viscous, buffer, and beginning of the logarithmic region. However, in contrast with this situation next to the wall, there is a general tendency to spectral convergence at the center of the channel. Based on the spectra of the fluctuations of the pressure field, it appears that one can conclude that such actions next to the wall and at the center region are driven by the pressure field. It is speculated, however, that the commented convergence at the center region can be greater for higher Reynolds numbers than that used in the present work.

1 INTRODUCTION

Turbulent heat transfer is a phenomenon of fundamental interest and technological relevance to a range of mechanical, aerospace, and chemical engineering processes in addition to a range of applications encountered in physics, biological and environmental sciences. Nevertheless, heat transfer predictions for most applications in practice utilize simplistic approaches based on Reynolds analogy, which implies similarity between momentum and heat transfer. This approach is computationally efficient since heat transfer predictions are essentially obtained from the turbulent velocity field at relatively little additional computational cost. However, most flows encountered in practice are far from equilibrium, the direct analogy between momentum and heat transfer fails, and use of the Reynolds analogy for predicting turbulent heat transfer can be very inaccurate (Spalart and Strelets, 2000; Kong, Choi, and Lee, 2001; Inaoka, Yamamoto, and Suzuki, 1999). Previous works show that there is a clear need to examine in detail the dissimilarities between heat and momentum transfer in non-equilibrium turbulent flows.

But in order to understand heat and momentum dissimilarity in non-equilibrium turbulent flows, however, it seems appropriate first, starting from previous results in the literature, look at this phenomenon in fully developed turbulent flow, trying to understand the way axial velocity and temperature correlates in this kind of turbulence. And also trying to see more deeply how this correlation degrades from high to lower values, from the wall toward the center region of the flow.

Similarity or dissimilarity between momentum and heat transfer means, similarity or dissimilarity between axial velocity and temperature fluctuations. The correlation between these fluctuations in wall bounded turbulent flow has been intensively investigated in the last three decades, first experimentally and then numerically. And as it has been shown in the literature with experimental works (Bremhorst and Bullock 1970; Orlando, Moffat, and Kays, 1974; Zaric 1975; Fulachier and Dumas, 1976; Hishida and Nagano 1979; Iritani, Kasagi, and Hirata 1985; Antonia, Krishnamoorthy, and Fulachier 1988), and numerical works (Kim and Min, 1989; Kasagi, Tomita, and Kuroda, 1992; Kawamura, Abe, and Matsuo 1999; Na, Papavassiliou, and Hanratty 1999; Na, and Hanratty 2000; Kong, Choi, and Lee 2000, and Kong, Choi, and Lee 2001), the similarity between the axial velocity and temperature fields, is very strong in the viscous and buffer region of a turbulent boundary layer. In those cases, for instance, with similar boundary conditions for the axial momentum and thermal fields, the normal fluxes of axial momentum and heat have the same direction, and the similarity is stronger. Although some minor differences in the first experimental works, nowadays it is known that the correlation coefficient is almost 1 next to the wall, decreasing as the the distance from the wall increases.

In order to justify this strong correlation between fluctuations of axial velocity and temperature, in previous works some explanations have been given based on the kind of turbulence structures that exists in the wall layer. Nowadays it is known that turbulence, and moreover bounded turbulence, has a high degree of organization (Kline, et al. 1967; Kim, Kline, and Reynolds 1971; Nychas, Hershey, and Brodkey, 1978; Swearingen and Blackwelder 1987; Corino and Brokey 1969; Hamilton, Kim, and Waleffe, 1995), and it has been some attempts to explain this close behavior of axial velocity and temperature on the wall layer based on coherent structures and intermitency. For example Bremhorst and Bullock (1970) has noted that the structures of velocity and temperature have a high degree of correlation next to the wall. And Orlando et al. (1974) suggested that the strong axial velocity and temperature correlation can be explained based on the long time identity of the near wall structures. Also Zaric (1975) trying to explain this similarity, computed the probability density function of axial velocity and temper-

ature, splitting the flow in a background turbulence and an intermittent phase in the wall layer. And Antonia, Krishnamoorthy, and Fulachier (1987), have speculated that the joint probability function of axial velocity and temperature fluctuations, from data in the viscous layer, reflect the presence of longitudinal vortices which lie on either side of the low-speed streaks next to the wall. These last authors, as also Fulachier and Dumas(1976) in a previous work, have used spectral analysis of axial velocity and temperature fluctuations. In Antonia et al's paper the spectral analysis is limited to the buffer and beginning of the logarithmic region. In this region they found that as the distance from the wall increases spectras became less and less similar, but in contrast next to the wall these differences disappeared. This last work was a kind of extension of Fulachier and Dumas's paper, who used also spectral analysis to study temperature and velocity fluctuations similarity in a boundary layer. Fulachier and Dumas' main conclusions were that afar from the wall there was a better correlation between temperature and the velocity vector, rather than axial velocity. Also they have suggested that temperature spectra has afar from the wall a closer behavior to normal velocity spectra, rather than to axial velocity.

The main focus of the present paper is to analyze the natural dissimilarity of fluctuations of axial velocity and temperature in the wall layer. The data are generated with a DNS of a fully developed turbulent channel flow with heat transfer. The scalar field is solved using a uniform energy source case. As regarding the Pr number, due Pr plays an important role in the limit of heat and momentum similarity (Na and Haritonidis 2000), most results in this paper are for $Pr = 1$, avoiding Prandtl number effects on dissimilarity. In the first part of the paper a short detail of the numerical procedure is given, and then results that show the strong correlation between u' and θ' commented above are presented. In the second part of the paper the importance of the most energetic events in the wall layer, in u' and θ' dissimilarity is presented. Then the spectral density functions of the fluctuations of velocity components, pressure and temperature fields are used in order to explain the possibles causes of u' and θ' correlation degradation afar from the wall. Then at the end the main conclusions are given.

2 NUMERICAL PROCEDURE

In this section a short description of the numerical aspects is presented. In Pasinato, and Squires (2006) a validation of the DNS of developed channel flow with heat transfer is presented. In this paper, u, v, and w are the instantaneous velocities in the streamwise (x), wall-normal (y), and spanwise (z) directions, respectively. All instantaneous variables are decomposed in a mean value and a fluctuation; e.g. $u = U + u'$. And the root mean square of any fluctuation is denoted with a plus symbol; e.g. u^+ for u'. Also it is used the plus symbol in order to denote nondimensionalization with the wall parameters, u_τ and ν; e.g. $y^+ = y\, u_\tau/\nu$.

A DNS of a turbulent channel flow with periodic boundary condition in x and z was performed. The computational domain is shown in Figure 1. The governing equations in dimensionless form are the continuity, the unsteady Navier-Stokes and the energy equations for incompressible flow and heat transfer,

$$\frac{\partial u_i}{\partial x_j} = 0 \tag{1}$$

$$\frac{\partial u_i}{\partial t} + \frac{\partial}{\partial x_j} u_j u_i \;=\; \frac{1}{R_\tau} \frac{\partial^2}{\partial x_j \partial x_j} u_i \;-\; \frac{\partial p}{\partial x_i} \tag{2}$$

$$\frac{\partial \theta}{\partial t} + \frac{\partial}{\partial x_j} u_j \theta \;=\; \frac{1}{Pr R_\tau} \frac{\partial^2}{\partial x_j \partial x_j} \theta \;+\; S_e \tag{3}$$

where the non-dimensionalization was done using the friction velocity v_τ and half channel distance between walls δ, and the friction temperature $T_\tau = q_w / \rho \, c_p \, u_\tau$. Where θ is the dimensionless temperature, q_w is the heat flux at the wall, and c_p and ρ are the constant pressure specific heat coefficient and the density, respectively. In these equations Pr, and R_τ are the molecular Prandtl and turbulent Reynolds numbers based on the v_τ wall friction velocity and half channel distance between walls δ, respectively, and S_e is a dimensionless energy source term.

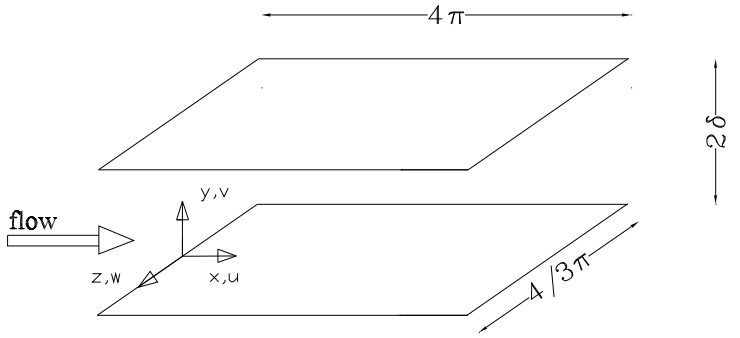

Figure 1: Computational domain for fully developed turbulent channel flow.

The computational domain is equal to 4π and $4\pi/3$ (1885, and 628 in wall units) in x and z directions, respectively. This computational domain is discretized with a $128 \times 128 \times 128$ grid, which in wall units means $\Delta x^+ = 14.72$, $\Delta y^+ = 0.09 - 6.72$, and $\Delta z^+ = 4.90$, in the three directions respectively. The time step was $0.0008\delta/u_\tau$ or $0.12\nu/u_\tau^2$.

The unsteady Navier-Stokes equations were solved numerically at a Reynolds number R_τ equal to 150. The numerical code used in the present work for the velocity fields was originally developed by Prof. Kyle Squires' group at ASU. In this code the incompressible momentum equation are discretized by the second-order accurate central-difference scheme. For the DNS with periodic boundary condition, the Poisson equation for the pressure field is Fourier-transformed with respect to the streamwise and spanwise periodic directions and the resulting three-diagonal equations are solved directly for each time step. The flow field is advanced in time using a fractional-step method, with the Crank-Nicolson second-order scheme for the viscous terms and the Adams-Bashforth scheme for the non-linear terms. The thermal field is solved with a numerical code with the same space, and time discretization, and the same scheme used for the flow field.

Periodic boundary conditions are used for the homogeneous direction x, and z, streamwise and spanwise, respectively, and non-slip boundary conditions at both walls. As initial condition, an instantaneous velocity field of a developed turbulent flow was supplied from a previous calculation for a turbulent channel flow with the same DNS code.

After the velocity field is calculated at each time step, the temperature field was obtained integrating the energy equation. Any buoyancy effect was neglected, thus temperature was considered as a passive scalar. For temperature a uniform heat source was used. The uniform

scalar source case solved in the present work is similar to case I solved in Kim and Moin (1989), who used a source term equal to $2/Re_\tau Pr$. In the present study, however, the source is a constant energy source uniformly distributed in the domain, equal to q_w/δ. Thus, in this case the dimensionless temperature $\theta = (T_w - T)/T_\tau$ is zero at the walls, and the dimensionless source $S_e = 1$. As initial conditions for the thermal field a developed thermal field from a previous calculation was giving. The statistics time integration was taken equal to $32\delta/u_\tau$, $40,000$ computational time step approximately, or $3,600\nu/u_\tau^2$, in order to define mean values.

3 RESULTS AND DISCUSSION

It is worth to mention that for the special case of $Pr = 1$ the Reynolds averaged form of equations (2-3) are,

$$\frac{\partial}{\partial x_j}(U_j U_i) = \frac{1}{R_\tau}\frac{\partial^2 U_i}{\partial x_j \partial x_j} - \frac{\partial}{\partial x_j}\langle u_i' u_j' \rangle - \frac{\partial P}{\partial x_i} \tag{4}$$

$$\frac{\partial}{\partial x_j}(U_j \Theta) = \frac{1}{R_\tau}\frac{\partial^2 \Theta}{\partial x_j \partial x_j} - \frac{\partial}{\partial x_j}\langle \theta' u_j' \rangle + S_e \tag{5}$$

where in these equations the source terms $-\partial P/\partial x_i$ and S_e are equal to 1 in dimensionless form.

Thus in this work for analysis porpoise of the special case with $Pr = 1$, the difference between axial velocity and temperature is defined as a new variable $\phi = u - \theta$, and used as measure of dissimilarity, where $\phi = \Phi + \phi' = (U - \theta) + (u' - \theta')$ as all variables. Also it is used the variance of ϕ normalized by the product of the root mean square of the fluctuations of axial velocity and temperature, u^+, θ^+, as a normalized measure of mean dissimilarity,

$$VAR_{\phi,norm} = \frac{\langle \phi^2 \rangle}{u^+\theta^+} = \frac{\langle uu \rangle - \langle u\theta \rangle}{u^+\theta^+} + \frac{\langle \theta\theta \rangle - \langle u\theta \rangle}{u^+\theta^+} \tag{6}$$

which is zero when $\rho_{u\theta} = 1$.

It is used this measure of dissimilarity, because it seems easier to look at an instantaneous measure like as $\phi' = u' - \theta'$, rather than to a product $u'\theta'$ of these fluctuations.

3.1 Longitudinal velocity and temperature correlation

(a)Mean values: In this item mean values taken in space and time for the homogeneous $x - z$ plane are presented. Figure 2(a) shows the normal to the wall distribution of $\rho_{u\theta}$, ρ_{-uv}, and $\rho_{-v\theta}$, the Reynolds and thermal stresses, the second moments $\langle uu \rangle$, $\langle u\theta \rangle$, and $\langle \theta\theta \rangle$, and the normalized variance of ϕ. The results in this figure confirm the strong similarity between the axial velocity and temperature fields in the wall layer, as it was commented in the introduction. The values presented here agree very well with the DNS results presented by Kasagi, Tomita and Kuroda(1992), as it is shown in the Figure, and with Kim and Moin (1989)'s results for a channel flow, and Kong, Choi, and Lee (2001)'s results for a boundary layer. These results also agree with the experimental data of Antonia, Krishnamoorthy, and Fulachier (1988), although in this last work the correlation coefficient has its maximum equal to 1 at the wall. In Figure 2(a), $\rho_{u\theta}$ has a values of 0.95 at the wall, a local maximum approximately at $y^+ = 5$ equal to 0.97 and a local minimum at the center of the channel equal to 0.58.

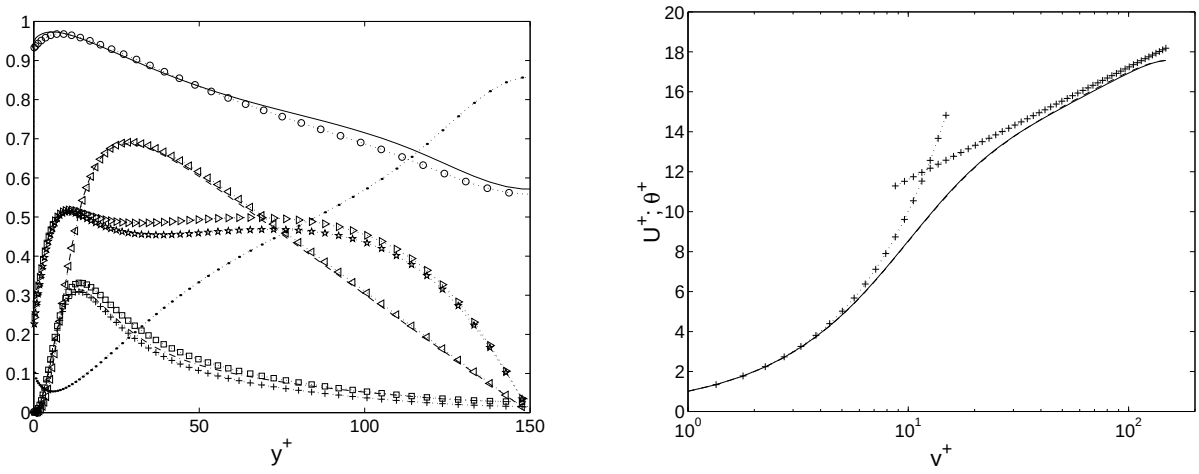

(a) (b)

Figure 2: (a) Wall normal distribution of second moments and correlation coefficients, for developed turbulent channel flow with $Re_\tau = 150$. Solid line, $\rho_{u\theta}$; $\circ \cdots \circ \cdots \circ$, $\rho_{u\theta}$ from Kasagi et al. (1992); $\cdots\cdots$, $VAR_{\phi,norm}$; $-.-.-$, $0.05 \times \langle u'\theta' \rangle$; $+\cdots+\cdots+$, $0.05 \times \langle u'u' \rangle$; $\square\cdots\square\cdots\square$, $0.05 \times \langle \theta'\theta' \rangle$;$*\cdots*\cdots*$, $\rho_{-v\theta}$; $- - -$, $-\langle v'\theta' \rangle$; $\rhd \cdots \rhd \cdots \rhd$, $\rho_{-u'v'}$; $\lhd \cdots \lhd \cdots \lhd$, $-\langle u'v' \rangle$. (b) Distribution of mean velocity and temperature for the uniform energy source case with $Pr = 1$ and $S_e = 1$. Solid line, mean velocity; $- - -$, mean temperature;$+\cdots+\cdots+$, $U^+ = y^+$ and $ln(y^+)/0.41 + 6.0$.

The conservation law for ϕ, from equations (2-3), Reynolds averaged for a fully developed turbulent channel flow is,

$$0 \;=\; \frac{1}{R_\tau}\frac{d^2\Phi}{dy^2} \;-\; \frac{d}{dy}(\langle u'v' \rangle - \langle v'\theta' \rangle) \tag{7}$$

Equation (7) shows that the dissimilarity in the mean velocity and temperature is different from zero if the wall normal gradient of the difference of the normal fluxes is different from zero. From Figure 2(a) it is seen that these normal fluxes are only slightly different from zero through the logarithmic sub-layer. And as it is shown in Figure 2(b), both the mean axial velocity and temperature have almost the same distribution. As regarding this slight difference between normal fluxes, on the other hand, it is worth to mention that is not possible to be sure how much of it is physical and how much is numeric. In other words, the instantaneous spatial and temporal gradients in the energy equation always are larger than those in the axial momentum equation as a consequence of the pressure gradient in the last equation. The same is to say that the energy equation is less stable in the numerical sense (Akselvoll and Moin, 1995). Thus the numerical resolution of the energy equation should have larger numerical errors, if the same numerical scheme is used in both equations.

Figures 3(a) and 3(b) show the two-point correlations coefficient with streamwise, and spanwise separation of velocity components and temperature, R_{uu}; R_{vv}; R_{ww}, $R_{\theta\theta}$, at four positions from the wall, $y^+ = 4,\ 16,\ 38,\ 116$. Once again these Figures, as commented previously, clearly show the strong correlation of axial velocity and temperature in the viscous and buffer regions. Then afar from the wall, toward the center of the channel, there is a departure between axial velocity and temperature, as it is seen for $y^+ = 116$. Also from both first locations, at $y^+ = 4$ and 16, it is clear the presence of long streamwise structures in both fields, thermal and axial velocity. The two-point correlations in the spanwise direction, on the other hand, with its

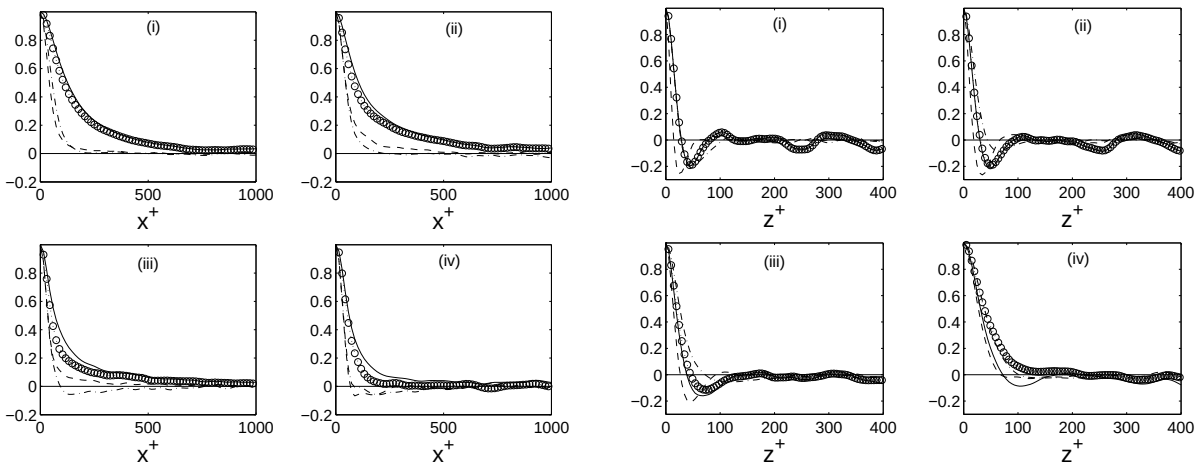

Figure 3: Two-point correlations coefficient. (a) Streamwise separation; (b) Spanwise separation. Solid line, u'; $\circ\cdots\circ\cdots\circ$, θ'; $---$, v'; $-.-.-$, w'. At four locations from the wall. (i) $y^+ = 4$, (ii) $y^+ = 16$, (iii) $y^+ = 38$, (iv) $y^+ = 116$.

minimum at $y^+ = 50$ in the viscous and buffer region, show the presence of streamwise vortices in these regions (Kline, et al. 1967; Kim, Moin, and Moser, 1987). In contrast, in the center of the channel this coefficient indicates a closer behavior of w and θ in the spanwise direction.

The results presented in this item indicate, as it is remarked in the literature, the u' and θ' close behavior in the viscous and buffer region. And a gradual de-correlation or increasing dissimilarity as the wall distance increases.

(b)Local statistics: In this item statistics of the serial time of the turbulent fluctuations are presented and discussed, at four positions from the wall.(1) $y^+ \simeq 4$, at the top of the viscous layer, which means approximately at the top of the low velocity streaky structure in the very near wall (Kim, Moin, and Moser, 1987; Hamilton, Kim, and Waleffe, 1995); (2) $y^+ \simeq 16$, at the buffer region where approximately occurs the maxims of velocity fluctuations; (3) $y^+ \simeq 38$, at the end of the buffer region and beginning of the semi-log region, where it is expected to be located approximately the top of the streamwise vortical structures in the wall layer, and (4) at $y^+ \simeq 116$, in the flow center region. The statistics time integrations was taken on time interval greater than $15,000\nu/u_\tau^2$ or $90\delta/u_\tau$ in all cases.

Statistics	$y^+ = 4$	$y^+ = 15$	$y^+ = 38$	$y^+ = 116$
S_u	0.64078	-0.17126	-0.54905	-0.53791
F_u	3.02714	2.18137	3.09128	3.53121
S_θ	0.70177	-0.11165	-0.45057	-0.72089
F_θ	3.13215	2.17178	2.81946	3.73155
S_ϕ	-0.30437	-0.02992	0.06042	0.17884
F_ϕ	5.94181	4.21981	3.45856	3.18046

Table 1: Skewness, S, and flatness,F, factors for $Pr = 1.0$, for u', θ', and ϕ' .

Figures 4(a) and 4(b) show the probability density functions, pdf, for axial velocity and

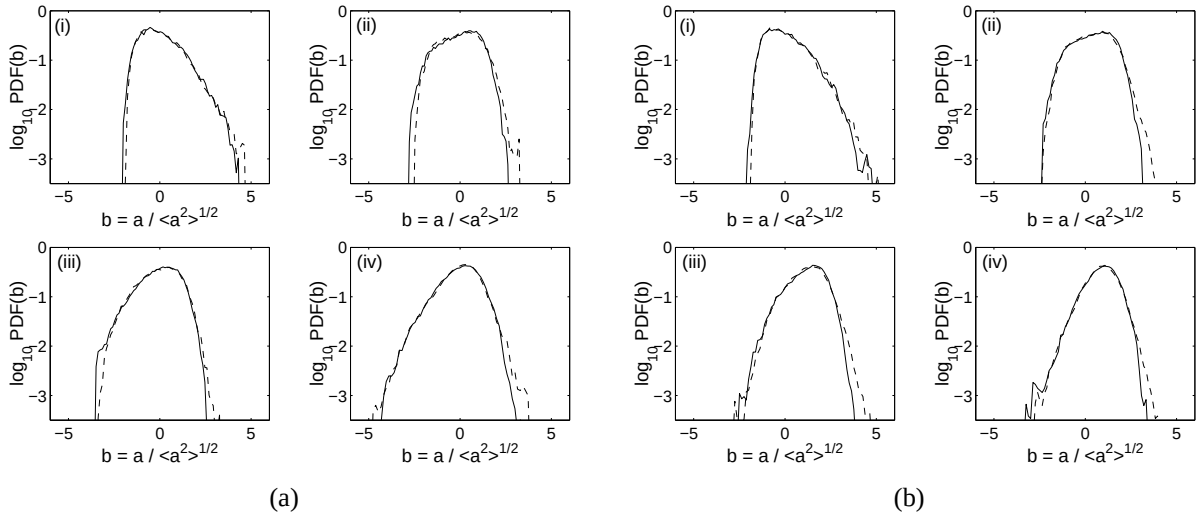

Figure 4: Probability density function of axial velocity and temperature at four positions from the wall, for two Prandtl numbers. Solid line $a = u'$; $- - -$ $a = \theta'$. (a) Pr=0.71; (b) Pr=1.0. (i) $y^+ = 4$; (ii) $y^+ = 16$, (iii) $y^+ = 38$, (iv) $y^+ = 116$.

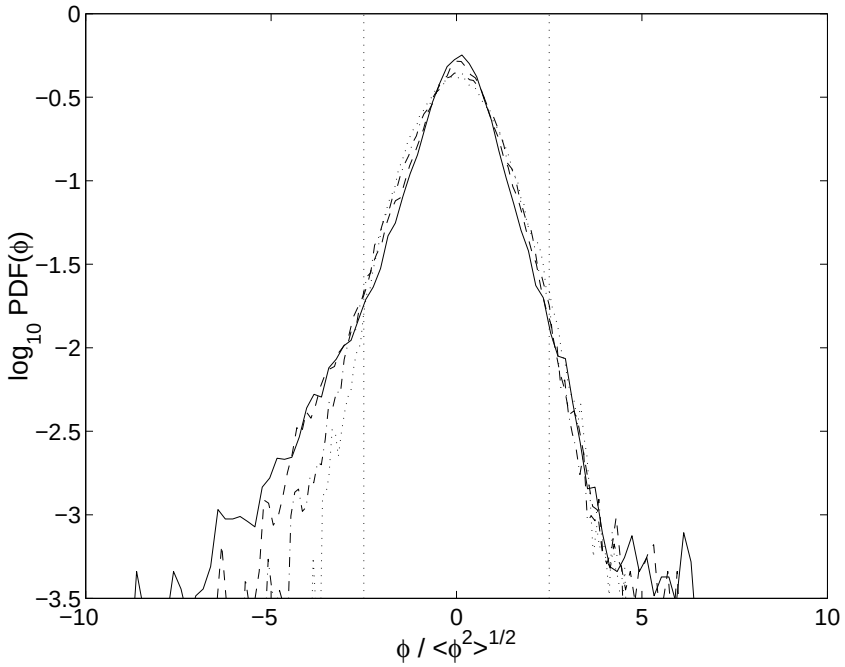

Figure 5: Probability density function of axial velocity and temperature difference, ϕ', for $Pr = 1$. Solid line $y^+ = 4$; $- - -$ $y^+ = 16$; $-.-.-$, $y^+ = 38$; $\cdots\cdots$, $y^+ = 116$. Vertical lines denotes $\phi/ < \phi^2 >^{1/2} = \pm 2.5$.

temperature fluctuations for $Pr = 0.71$ and 1, at the four positions from the wall. And Table 1 show the skewness factor, S, and flatness factor, F, for u', θ', and ϕ' at the four positions. S is positive in the viscous layer, and negative in both variables in the other locations. Both pdf are almost symmetric for the second and third locations, at the buffer region and beginning of the logarithmic sublayer. They show, however, that for very large values of u' its pdf $p(u)$ is smaller than $p(\theta)$ in the four positions. These last results are consistent with experimental results in the literature (Antonia, Krishnamoorthy, and Fulachier 1988; Zaric 1975). They show also that for very low values of u', the $p(u)$ is slightly greater than the $p(\theta)$ in the first three locations near the wall, and almost the same in the center of the channel.

Thus the main characteristic of these figures is that the fluctuations of temperature are always slightly larger than velocity fluctuations. When fluctuations are positive, the absolute value of the temperature fluctuations are larger, and when fluctuations are negative, the absolute values of the temperature fluctuations are smaller. In this work u and θ have the same boundary conditions, therefore, positive fluctuations means inrush or sweeping movements of warm fluid with high momentum toward the wall. Thus Figures 4(a) and 4(b) show that for those warm high momentum movements toward the wall, temperature experiment stronger oscillations than velocity. In contrast, for the ejections of cold fluid with low momentum from the near wall region toward the center of the channel, u fluctuations are stronger.

Figure 5, which shows the pdf for the fluctuation of axial velocity and temperature difference, ϕ', for the four positions from the wall for $Pr = 1$, shows also the same difference in negative and positive u and θ fluctuations. In other words, the correlation between u and θ is for positive u' and positive θ'. There are only few events where these fluctuations have opposite sign. Thus, $\phi' < 0$ means sweeping motions, and $\phi' > 0$ ejections. And Figure 5 shows, and the same can be seen from S_ϕ factor in Table 1, larger $p(\phi)$ of negative fluctuations in ϕ in the wall layer. Thus sweeping motions are more frequent than ejections next to the wall. Another aspect in this figure is that pdf of ϕ' seems to be the results of two kind of flow, a background turbulence and an intermittent phase, like as it was taken by Zaric (1975) in his paper. One phase for ϕ' in the interval $\pm 2.5\phi^+$ (where ϕ^+ means the rms of ϕ), which can be associate with a calm period of flow. And a second phase for $|\phi'| > 2.5\phi^+$, for abrupt events like as ejections or sweeping motions. That ϕ can reflect these two phase of turbulence is not a surprise, since it is the instantaneous dissimilarity. In the last subsection this result is used as a criteria to detect the dissimilarity in amplitude that cause the most energetic events at the wall layer.

More details of the u' and θ' correlation degradation from the wall toward the center of the channel can be extracted from the joint probability density function, jpdf, of both variables. Figures 6(a), and 6(b) show the jpdf for u' and θ', for the four positions from the wall, for $Pr = 0.71$, and $Pr = 1.0$. Note that it was used a difference in scales. The results for $Pr = 0.71$ show the effect of the lower Pr for all fluctuations at the viscous layer, and basically for negative fluctuations at the buffer region. In other words, for those fluctuations coming from the cold low momentum flow near the wall, where molecular transfer of momentum and heat are important. Note that fluctuations in these Figures are not normalized by the rms. Based on the fact that correlation equal 1 is a linear function, Figures 6(b)-a to d, clearly show how correlation change from high values at the viscous layer to more or less a half at the center of the channel.

Same last results are presented in this subsection based on two-point correlation. They are the comparison of the patterns of the two correlations: skinfriction-streamwise vorticity, and wall heat transfer-streamwise vorticity. Some works have been published related with drag reduction, where it was found that regions of high skin-friction at the wall are related with the

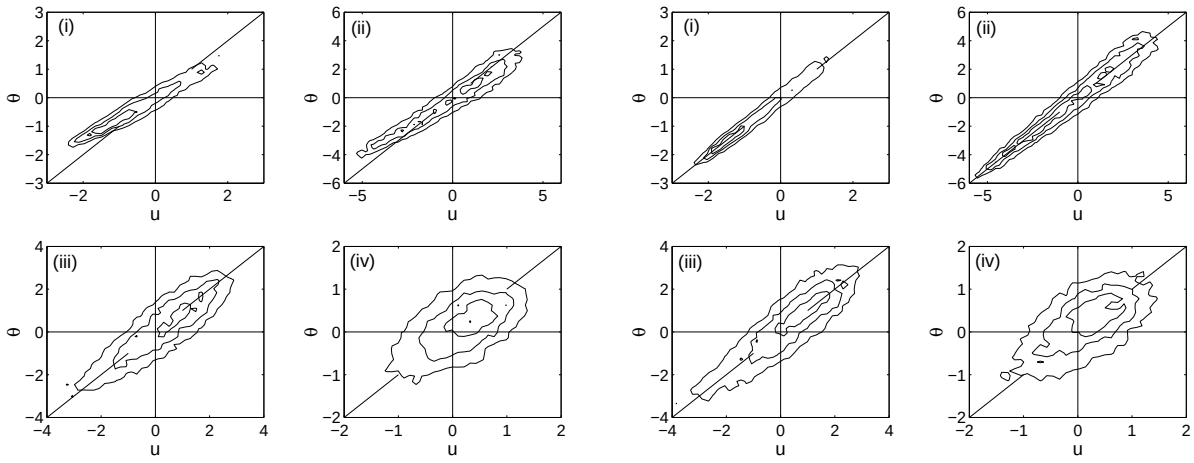

Figure 6: Joint probability density function of axial velocity and temperature at four positions from the wall, for two Prandtl numbers. (a) Pr=0.71; (b) Pr=1.0. (i) $y^+ = 4$; (ii) $y^+ = 16$, (iii) $y^+ = 38$, (iv) $y^+ = 116$. Note the different scales in (i, ii, iii, and iv). Contour levels are in the interval $0 - 0.01$ with increment of 0.0033 in (a), and in the interval $0 - 0.015$ with increment of 0.005 in (b). Diagonal solid lines denote 45 degree tangent linear functions.

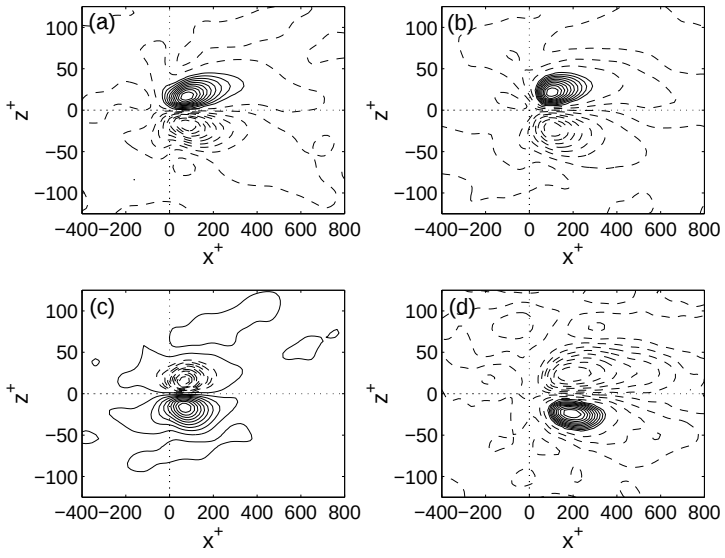

Figure 7: Two-point normalized correlation $Q(r_x, y, r_z)$ between the wall shear rate and streamwise vorticity, in the plane (x^+, z^+) at four positions from the wall. (a) $y^+ = 0.016$, (b) $y^+ = 4$, (c) $y^+ = 16$, (d) $y^+ = 38$. Contour levels are in the rage $-2.5, +2.5$ with increments of 0.25. Positive and negative contours are represented by solid and brokenlines, respectively. Doted lines denote detection point at the wall.

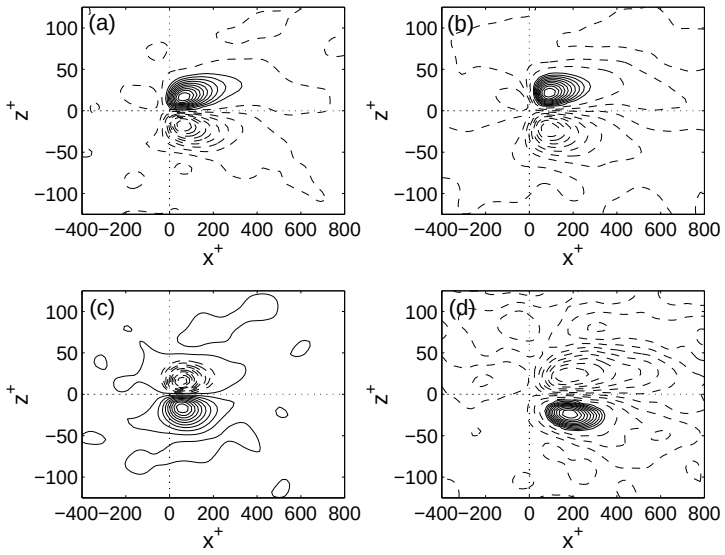

Figure 8: Two-point normalized correlation $Q(r_x, y, r_z)$ between the wall heat rate and streamwise vorticity, in the plane (x^+, z^+) at four positions from the wall. (a) $y^+ = 0.016$, (b) $y^+ = 4$, (c) $y^+ = 16$, (d) $y^+ = 38$. Contour levels are in the rage $-2.5, +2.5$ with increments of 0.25. Positive and negative contours are represented by solid and brokenlines, respectively. Doted lines denote detection point at the wall.

presence of streamwise vortical structures in the buffer region. First Choi, Moin, and Kim(1993) have shown that regions of high skin-friction are associated with streamwise vortices right above the wall. Then Kravchenko, Choi, and Moin(1993) shown that skin-friction correlates with near-wall streamwise vortices.

Here the same kind of two-point correlation used by Kravchenko et al. was used for the instantaneous wall normal gradient of u and θ, with the instantaneous streamwise vorticity. The objective of these results was to compare the gross pattern of these correlations. Note that in this work the correlations are normalized. The two-point correlations were evaluated from 24 instantaneous flow fields with $Pr = 1$, that were equally separated in time $30,0\nu/u_\tau^2$. These correlations are,

$$Q(r_x, y, r_z) = \frac{\langle A(x, y_d, z)\omega_x(x + r_x, y, z + r_z)\rangle}{\omega_x^+} \tag{8}$$

where (x, y_d, z) is the detection point and $(x + r_x, y, z + r_z)$ the second point, A is equal to $(\partial u'/\partial y)(x, y = 0, z)$ for the skin-friction, and to $(\partial\theta'/\partial y)(x, y = 0, z)$ for wall heat transfer, and $\langle\ \rangle$ denotes averaging in x, z, and time.

In this paper only a few results for these correlations are shown in Figures 7 and 8, where they clearly show that normal temperature gradient at the wall correlates with streamwise vorticity in almost the same way that wall normal gradient of axial velocity does.

More results using this two-point correlation technique, with ϕ' at the detection point (x, y_d, z) and the streamwise vorticity $\langle\phi(x, y_d, z)\omega_x(x + r_x, y, z + r_z)\rangle$, or the wall normal velocity, $\langle\phi(x, y_d, z)v(x + r_x, y, z + r_z)\rangle$, among other variables were calculated. And these correlations were evaluated for different positions of the detection point, at $y^+ = 4, 16, 23, 38$. The most interesting results from these correlations, that will be reported elsewhere, is that dissimilar-

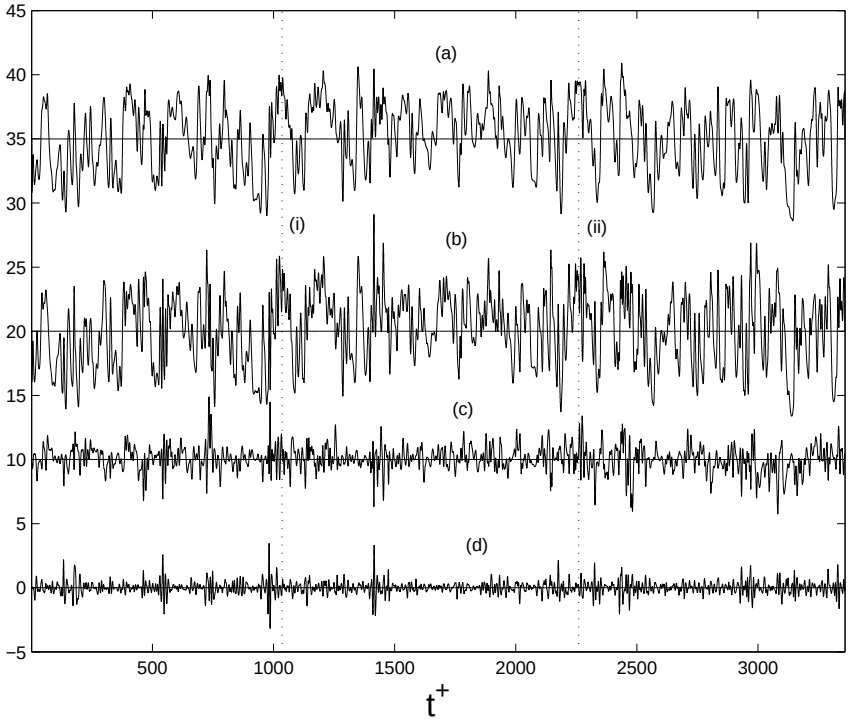

Figure 9: Sample of filtered instantaneous fluctuations. (a) $u' + 35$; (b) $\theta' + 20$; (c) $\phi' + 10$, (d) $(\partial p'/\partial x^+) \times 10$. Vertical dots denote two particular events.

ity occurs basically between two regions with opposite streamwise vorticity in $x - z$ planes, and that it correlates basically with negative wall normal velocity in region immediately above the detection point. This region with negative wall normal velocities is a vertical and narrow region that begins near the center of the channel. These results give more support to the speculation that dissimilarity is mainly associated with sweeping movements of warm flow with high momentum toward the wall.

3.2 Mean contribution to dissimilarity from most energetic events

Figure 9 shows a sample with the filtered instantaneous u', θ', ϕ', $(\partial p'/\partial x)$ at $y^+ = 16$. In order to filter the fluctuations a moving mean was applied, using a short period of time, $T^+ = tu_\tau^2/\nu = 3.6$, in comparison with the period of time of the most energetic events like as sweeping or ejection motions near the wall (Luchik and Tiederman, 1987; Shah and Antonia 1988).

An interesting aspect in Figure 9 is that, eventually, there are events in which u' and θ' clearly show different behavior. For instance, in the events denoted as (i) and (ii), temperature fluctuations present, superimposed, small amplitude oscillations of high frequencies, at the extremes of the main fluctuations. In contrast, these high frequency oscillations look almost dumped in the axial velocity fluctuations. On the other hand, this Figure clearly shows, as it was expected, that exists an association of the strongest dissimilarities, or big oscillations in ϕ, with the most energetic events in the axial gradient of p' in the major part of the sample. It is also important to remark that ϕ' clearly presents, as it was also expected, two phases. One associated with the important oscillations of the flow, and other more calm, where dissimilarity

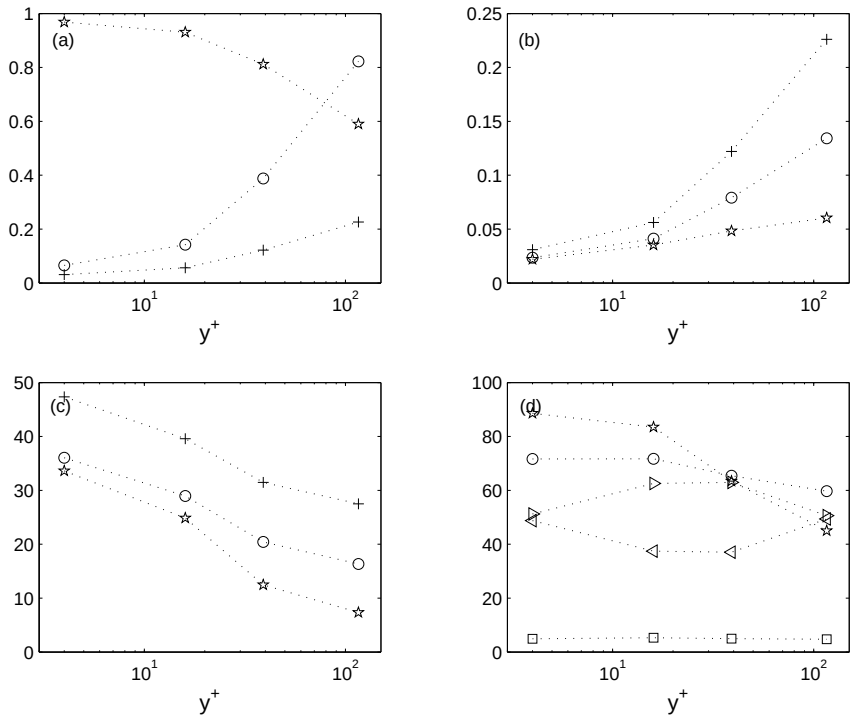

Figure 10: Contribution to dissimilarity of the most energetic events in the wal layer. (a) $*\cdots*\cdots*$, $\rho_{u\theta}$; $\circ\cdots\circ\cdots\circ$, $VAR_{\phi,norm}$; $+\cdots+\cdots+$, $VAR_{\phi,norm}$ from events that satisfy condition (9). (b) $VAR_{\phi,norm}$ from events that satisfy the following conditions: $+\cdots+\cdots+$, condition (9); $\circ\cdots\circ\cdots\circ$, condition (11); $*\cdots*\cdots*$, condition(12). (c) Same as in (b) but $VAR_{\phi,norm}$ as $\%$ of total $VAR_{\phi,norm}$. (d) Events with the following conditions in $\%$. $\square\cdots\square\cdots\square$, condition (9) over the whole sample; $\circ\cdots\circ\cdots\circ$ condition (11) over events that satisfy (9); $*\cdots*\cdots*$, events that satisfy (12) of events that satisfy (11); $\triangleleft\cdot\triangleleft\cdot\triangleleft\cdot\triangleleft$, events that satisfy condition (13) of events that satisfy (9); $\triangleright\cdots\triangleright\cdots\triangleright$, events that satisfy (14) of events that satisfy (9).

presents high frequency and small amplitude. Thus it seems appropriate to find out the contribution to dissimilarity of the big oscillations, and those from differences in frequency. And this is presented in this and next subsection.

Thus the idea in this subsection is to detect events characterized as *important dissimilarity event* with some algorithm and evaluate their mean contribution to the mean dissimilarity, as it was defined in equation (6). As detection algorithms for an *important dissimilarity event* one analogous to those used in the literature to detect burst or ejection events, was used. The most common of these algorithms are the uv quadrant 2, the variable interval time average (VITA), and the $u-$label techniques. And they have been used in order to investigate burst period and high pressure peaks frequency in wall turbulence(Lu and Willmarth, 1973; Blackwlder and Haritonidis, 1983; Luchik and Tiederman, 1987; Shah and Antonia 1988; Johansson, Her, and Haritonidis 1987). In this work, however, the idea is not to relate the most important instantaneous oscillations in ϕ with events like as burst, ejections or sweeping motions. Rather than the objective is only to identify the most energetic events in the wall layer. And then to evaluate their importance in the production of axial velocity and temperature mean dissimilarity, no matter they are burst, ejections or sweeping motion events. And no matter if an events like as

an ejection is split out in two or more events.

Then the algorithms used to detect important dissimilarity events, based on the VITA and the second quadrant algorithms, detect one events when the variance of ϕ is,

$$\widehat{\phi'^2} - \bar{\phi}^2 \ \geq \ k\phi^+ \tag{9}$$

where as mean values for ϕ the mean values of the whole sample is used, which is almost zero for the thermal case solved here, and the wide-hat symbol means a mean values in the time filtering interval T,

$$\widehat{\phi(t,T)} \ = \ \frac{1}{T}\int_{t-T/2}^{t+T/2} \phi'(\tau)d\tau \tag{10}$$

The algorithms above have two parameters, the filtering time period T and the threshold k. k was taken equal 2, as a conservative value based on the pdf of ϕ (values of ϕ out of the interval $\pm 2.5\phi^+$) in Figure 5. As regarding the second parameter, the period of filtering T, this period in dimensionless form used in this work was $T^+ = 1.2$, which is well out the range, $6 < T^+ = tu_\tau^2/\nu < 13$, for dimensionless burst period found in the literature. On the other hand, because the mean and the rms values of ϕ, ϕ^+ and $\bar{\phi}$, used in the algorithms are evaluated for the whole sample, the algorithms can be used for instantaneous values without any filter. Moreover, numerical tests were done which shown that results were only slightly sensible to the filtering period for values of $T^+ < 10$.

Therefore, using the algorithms above, once an event that qualify as important dissimilarity event was detected, conditional probability with different conditions were used in order to characterize whether these events with strong dissimilarity in axial velocity and temperature, satisfy a second, or a second and a third condition. Some of the conditions used were,

$$P(\widehat{\phi'^2} - \bar{\phi}^2 > k\phi^+, \widehat{u'v'} < 0) \tag{11}$$

aiming at to detect how many of the events detected as important dissimilarity events, also belong to events in the second quadrant, Q2.

$$P(\widehat{\phi'^2} - \bar{\phi}^2 > k\phi^+, \widehat{u'v'} < 0, \widehat{v'} < 0) \tag{12}$$

aiming at to detected events in Q2 and also with negative fluctuation of normal velocity.

$$P(\widehat{\phi'^2} - \bar{\phi}^2 > 2\phi^+, \widehat{\partial p'/\partial x} < 0) \tag{13}$$

$$P(\widehat{\phi'^2} - \bar{\phi}^2 > 2\phi^+, \widehat{\partial p'/\partial x} > 0) \tag{14}$$

aiming at to detect whether dissimilarity is associated with favorable or adverse instantaneous axial pressure gradient.

Figure 10 show some of the most relevant results. In first place, Figure 10-a shows the correlation coefficient $\rho_{u\theta}$, the total dissimilarity, equation (6), and the dissimilarity owing to those events that qualify as the most energetic events in the wall layer, at the four positions from the wall used in this work. The first conclusion from this figure is that the most energetic events are responsible of a part of total dissimilarity, but it is in the four locations less than a half of the total. In other words, as it is shown in Figure 10-c, the contribution of these big events to the total dissimilarity is alway smaller than 50% in the whole wall layer.

Hence, the main features of Figures 10-(a), (b) and (c), indicate, as it commented above, that the most energetic events have a part in dissimilarity, but the major contribution are due to another physical causes. On the other hand, this contribution to dissimilarity by the energetic events in the wall layer decreases toward the center of the channel. At the center of the channel its contribution is less than 30% of the total dissimilarity as it is shown by Figure 10-(c).

Figure 10-(d) shows the frequency of events detected as important dissimilarity event, with a second or a second and a third condition. It is seen that the inrushes or movements of high momentum toward the wall are felt in the whole flow, and that the number of events detected with this condition is more or less equal to 75% in the viscous layer, decreasing slowly afar from the wall. Looking now to the frequency of events that satisfy also a condition on the pressure gradient, the results show that at the viscous layer and at the center of the channel the important dissimilarity events are almost not related with the sign of the pressure gradient. On the other hand, the sign of the pressure gradient has, although slightly, an effect in the buffer region and in the beginning of the logarithmic sub-region. In this Figure 10-(d) is seen also that there are approximately a 70% of events that qualify as important dissimilarity events in the viscous layer, which are in the second quadrant $u'v' < 0$, and the 90% of them satisfy also $v' < 0$. Then both percentage decrease toward the center of the flow, and at the center region of the channel less than 50% of the $u'v' < 0$ events are also $v' < 0$ events. And a surprising result is seen from condition in equation (12), which detect those important dissimilarity event in the second quadrant that have negative normal velocity. The results in Figure 10-b show that in the viscous layer this kind of events are nearly the 90%. In other words, the most important dissimilarity events in the second quadrant are owing to sweeping motion and not to burst or ejections. Nevertheless, this percentage change quickly toward the center of the channel, where there the contribution of burst/ejection and sweeping motions to the most important dissimilarity events are almost the same.

In conclusion, therefore, the contribution to dissimilarity of the most energetic events in the wall layer is important, but do not explain the major causes of correlation degradation between axial velocity and temperature toward the center of the channel. Neither they explain the major fraction of dissimilarity in the viscous and buffer regions where these events are the strongest.

3.3 Spectral density functions

Figures 11 and 12 show the spectra for the fluctuations of velocity components, temperature, the difference between axial velocity and temperature, ϕ, and pressure, normalized by their rms, at four locations from the wall. Note the small difference of position of data at the center of the channel, Figures 11-d and 12-d, related to previous figures. The spectra for p' is in both Figures in order to improve comparison, and also because it is thought that p' has fundamental importance in the energy distribution among velocity components and thermal field. In order to obtain the spectra the data set, of approximately $19,000\nu/u_\tau^2$ in dimensionless time, was segmented into 92 segments with 1024 time-steps everyone. Then the periodograms were averaged together to obtain the spectral density function at 1024 frequencies. The segments were overlapped by one half of their length. On the other hand, for the frequency leakage the data were windowed with a Welch window. There were selected the four positions at $y^+ = 4$, 16, 38, and 126, because they give a more or less complete picture of the spectra modification in the wall layer. It is plotted the decimal logarithmic of $\omega\delta/u_\tau$ in the abscissa, and the product of $(\omega\delta/u_\tau)\Phi_a$ in ordinate, where Φ_a is the spectral density function of the variable a normalized to unity. The area under any section of Figures 11 and 12 is proportional to the fraction

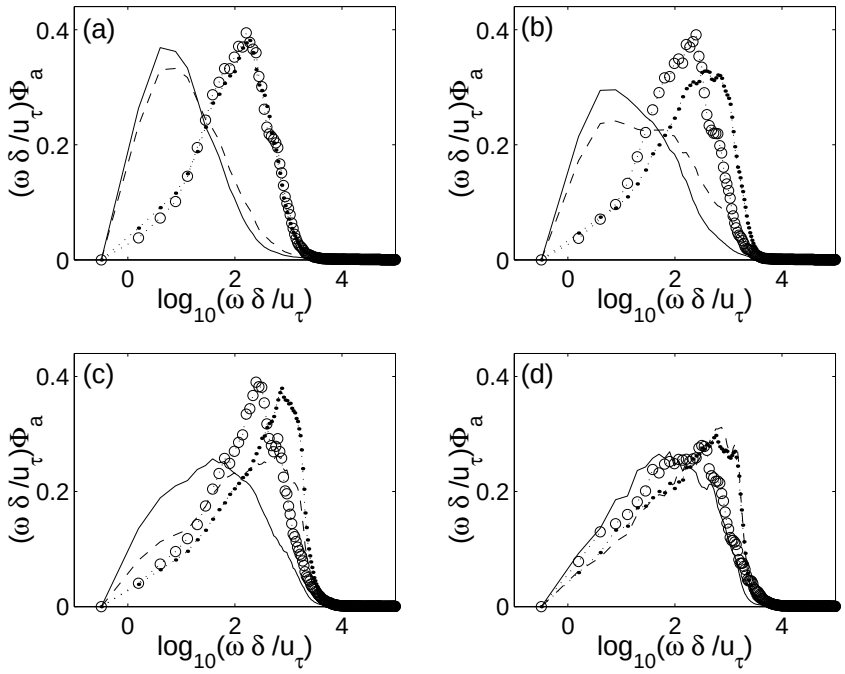

Figure 11: Spectral density function of u', θ', ϕ', and p', at four positions from the wall, (a) $y^+ = 4$; (b) $y^+ = 16$; (c) $y^+ = 38$; (d) $y^+ = 126$. Solid line, $a = u'/u^+$; $- - -$, $a = \theta'/\theta^+$; $\cdots\cdots$, $a = \phi'/\phi^+$; $\circ\cdots\circ\cdots\circ$, $a = p'/p^+$.

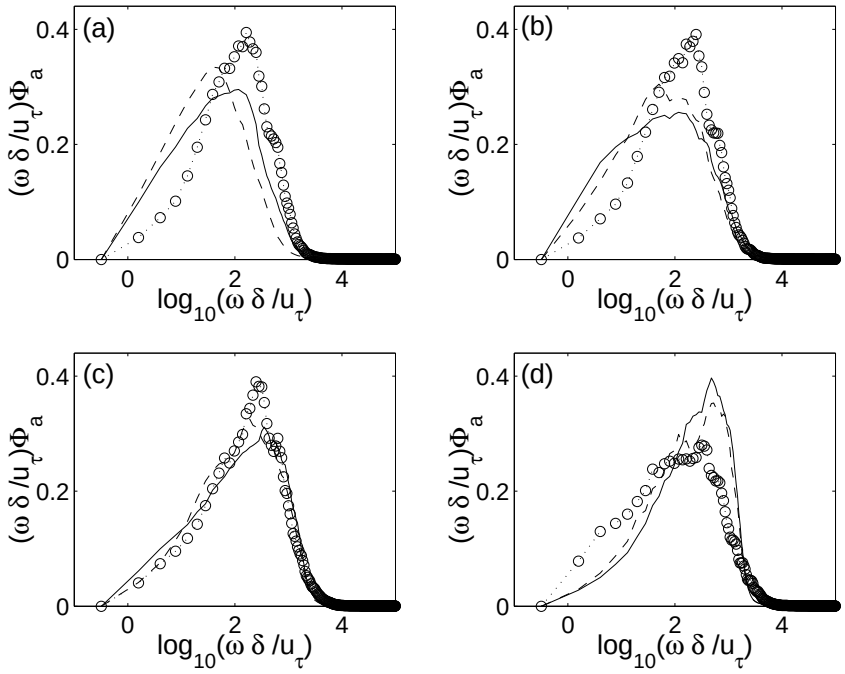

Figure 12: Spectral density function of v', w', and p', at four positions from the wall, (a) $y^+ = 4$; (b) $y^+ = 16$; (c) $y^+ = 38$; (d) $y^+ = 126$. Solid line, $a = v'/v^+$; $- - -$, $a = w'/w^+$; $\circ\cdots\circ\cdots\circ$, $a = p'/p^+$.

of total $\langle a'^2 \rangle / a^{+2}$ in that particular frequency range. In other words, spectra show the energy distribution of normalized fluctuations.

From these Figures it can seen from the spectra of u' and θ' at the four positions, that there is a shift toward higher frequencies of both spectras. But those in θ' is always greater, and this difference increases quickly in the first three positions from the wall. Then this difference decreases slightly toward the center region. In both spectras, as position y^+ increases for the first three positions, the peaks decreases as its position tends to shift toward higher frequency. This results agree with was found by Antonia et al. (1987), who did observations in a heated turbulent boundary layer for $y^+ < 40$. At the center of the channel the peaks if u' and θ' spectras increases as regarding those in the beginning of logarithmic layer, $y^+ = 38$. On the other hand, spectras for ϕ' and p' show that p and ϕ have a very similar spectra at the viscous region, $y^+ = 4$. Actually, they are almost the same in the whole extension. Then ϕ' spectra suffers a shift toward higher frequencies in comparison to p' spectra, but at the second and third position from the wall, buffer and beginning of the logarithmic regions, the peaks of ϕ' spectra shows a slight tendency toward lower frequencies. Then at the center of the channel, both spectras present the lowest peaks. Looking now to the spectras for v' and w' in comparison with p' spectra, they cleary show that there is a tendency of both velocity components spectra to follow those of p'. This tendency is maximum at the beginning of the logarithmic region $y^+ = 38$. Then at the center p' spectra shows a tendency toward lower frequencies, and its peaks has quickly decreased. And at the center of the channel also, unlike in the buffer and in the beginning of the logarithmic region, spectra of v' and w' present the steepest right tail. But most important, the right tails of v' and w' spectras are toward higher frequencies as regarding p' spectra.

One possible explanation for these behavior in spectra of fluctuations of turbulence is that the intermittent phase of turbulence introduces high frequency perturbations in the pressure field. And, because it is through the pressure field that such energy is redistributed among the different velocity components (Tennekes and Lumly 1976), these perturbations activate high frequencies in the normal and spanwise velocities. Moreover, this high frequency energy coming from the most energetic events in the wall layer is introduced into the scalar or thermal field through the convective terms, generating even higher frequencies, e.g. events i and ii at Figure 9. It seems that without any 'buffer' term like as the pressure gradient in the momentum equations, the energy equation generates higher gradient and thus faster oscillations on thermal field.

It is worth to note also that the spectras for p fluctuations at the four positions from the wall, have the peaks at almost the same frequency. Based on this result it appears that one can conclude that pressure field acts driving energy in velocity components, from low to high frequencies near the wall (in the viscous, buffer, and beginning of the logarithmic region), and in opposite direction in the center region. At the center of the channel pressure field drives energy toward lower frequencies in the momentum equations, and so on thermal field, enforcing a kind of spectras convergence in the center region. Although it is speculated that in the present paper there is only a small tendency to convergence owing to the lower Reynolds number, $Re_\tau = 150$. In this sense, it would be appropriate to check low Reynolds number effects in the present results.

Finally, it is important to remark that without the use of the new variable ϕ, it would be difficult to figure out how the difference in temperature and axial velocity fluctuations was conformed in the frequency domain. And, although it was expected it would be difficult, to link the origin of natural dissimilarity in the frequency domain to the action of v and w fluctuations

through the convective terms. Figure 11-a clearly shows that dissimilarity in the viscous region is driving by p fluctuations, through normal and spanwise velocity fluctuations.

4 CONCLUSION

In this paper the causes of natural dissimilarity of axial velocity and temperature in a turbulent channel flow were analyzed based on data generated by DNS. The temperature was considered as a passive scalar, and the thermal field is generated with a uniform energy source case.

The paper is thought to be a complement of previous contributions in the literature oriented to investigate correlation of temperature and longitudinal velocity fluctuations. It is mainly oriented to quantify the importance of the most energetic movements in the wall layer, those in the intermittent phase of turbulence, in the fluctuations of temperature and axial velocity dissimilarity. It is also oriented to present more evidences of spectral dissimilarity. For instance, the origin or causes of dissimilarity in the frequency domain, owing to the pressure field fluctuations and the action of wall normal and spanwise velocity fluctuations. And finally it shows that natural dissimilarity between axial velocity and temperature fluctuations has its major contributions from frequency domain.

Thus, the main conclusions from this work are that the most energetic events in the wall layer, as a consequence of sweeping and ejection motions, do not contribute significantly in a direct way to the de-correlation between axial velocity and temperature afar from the wall. The major part of dissimilarity occurs in the frequency domain. The natural dissimilarity in the wall layer increases afar from the wall, mainly owing to the shift toward higher frequencies of temperature fluctuations, in comparison with axial velocity fluctuations. Temperature spectra departs from those of axial velocity as the distance from the wall increases, but at the center region of the channel all velocity and temperature spectras show a tendency to convergence. And it is speculated that such action is driven by the fluctuations of the pressure field. It is thought that this convergence can be greater for higher Reynolds numbers. Therefore it would be appropriate to check the present results for higher Reynolds numbers.

ACKNOWLEDGMENT

This work was sponsored by the Air Force Office of Scientific Research under Grant No. FA9550-07-1-0393.

REFERENCES

[1] K. Akselvoll, and P. Moin. Large-Eddy simulation of turbulent confined coannular jets and turbulent flow over a backward facing step. Report TF-63, Thermoscience Division, Department of Mechanical Engineering, Stanford University, 1995.

[2] R.A. Antonia, H.Q. Danh and a. Prabhu. Response of a turbulent boundary layer to a step change in surface heat flux. *J. Fluid Mech.*, **80**, 153, 1977.

[3] R.A. Antonia and H.Q. Danh. Structure of temperature fluctuations in a turbulent boundary layer. *Physics of Fluids*, **20**(7), 1050-1057, 1977.

[4] R.A. Antonia. Behavior of the turbulent Prandtl number near the wall. *Int. J. Heat Mass Transfer*, **23**, 906-908, 1980.

[5] R.A. Antonia, L.V. Krishnamoorthy, and L. Fulachier. Correlation between the longitudinal velocity fluctuation and temperature fluctuation in the near-wall region of a turbulent boundary layer. *Int. J. Heat Mass Transfer*, **31**(4), 723-730, 1987.

[6] R.A. Antonia, L. Fulachier, L.V. Krishnamoorty, T. Benabid, and J. Anselmet. Influence of wall suction on the organized motion in a turbulent boundary layer, *Journal of Fluid Mechanics*. **190**, 217, 1988.

[7] K. Bremhorst, and K.J. Bullock. Spectral measurements of temperature and longitudinal velocity fluctuations in fully developed pipe flow, *Int. J. Heat Mass Transfer*. **13**, 1313-1329, 1970.

[8] H. Choi, P. Moin, and J. Kim. Direct numerical simulation of turbulent flow over riblets. *J. Fluid Mech.*, **255**, 503-539, 1993.

[9] L. Fulachier and R. Dumas. Spectral analogy between temperature and velocity fluctuations in a turbulent boundary layer. *J. Fluid Mechanics*, **77**, 257-277, 1976.

[10] Hamilton, J.M., J. Kim, and F. Waleffe Regeneration mechanism of near-wall turbulence structures. *J. Fluid Mech.*, **287**, 317-348, 1995.

[11] M Hishida, and Y. Nagano. Structure of turbulent velocity and temperature fluctuations in fully developed pipe flow, *J. Heat Transfer*. **101**, 15-22, 1979.

[12] J. Inaoka, J. Yamamoto, and K. Suzuki. Dissimilarity between heat transfer and momentum transfer in a disturbed turbulent boundary layer with insertion of a rod - modeling and numerical simulation. *Int. J. Heat Fluid Flow*, **20**, 290-301, 1999.

[13] Y. Iritani, N. Kasagi, and M. Hirata. Heat transfer mechanism and associated turbulence structure in the near wall region of a turbulent boundary layer, in *Turbulent Shear Flow*. **4**, 223-234, 1985.

[14] K. Kasagi Y. Tomita, and A. Kuroda. Direct numerical simulation of the passive scalar field in a turbulent channel flow. *Transaction of ASME, Journal of Heat Transfer*, **114**, 598-606, 1992.

[15] N. Kasagi and Y. Ohtsubo. Direct numerical simulation of low Prandtl number thermal field in a turbulent channel flow. In *Turbulent Shear Flow*, **8**, 97-119, 1993.

[16] H. Kawamura, H. Abe, and Y. Matsuo. DNS of turbulent heat transfer in channel flow with respect to Reynolds and Prandtl number effects. *Int. J. Heat Fluid Flow*, **20**, 196-207, 1999.

[17] J. Kim On the structure of wall-bounded turbulent flow, *Physics of Fluids*. **26**, 2088, 1983.

[18] H.T. Kim, S.J. Kline, and W.C. Reynolds, The production of turbulence near a smooth wall in a turbulent boundary layer *J. Fluid Mechanics*, **56**, 133-159, 1971.

[19] J. Kim, P. Moin and R. Moser. Turbulent statistics in fully developed channel flow at low Reynolds number. *J. Fluid Mechanics*, **177**, 133-166, 1987.

[20] J. Kim, and P. Moin. Transport of Passive Scalar in a Turbulent Channel Flow. In *Turbulent Shear Flow*, **6**, 86-96. 1989.

[21] H. Kong, H. Choi, and J.S. Lee.Dissimilarity between the velocity and temperature fields in a perturbed turbulent thermal boundary layer. *Physics of Fluids*, **13**(5), 1466-1479, 2001.

[22] A.G. Kravchenko, H. Choi, and P. Moin, On the relation of near-wall streamwise vortices to wall skin friction in turbulent boundary layer. *Physics of Fluids A*, **5**(7), 3307, 1993.

[23] Y. Na, D.V. Papavasiliou, and T. J. Hanratty. Use of direct numerical simulation to study the effect of Prandtl number on temperature fields. *Int. J. Heat and Fluid Flow*, **20**, 187-195, 1999.

[24] Y. Nagano and M. Tagawa. Statistical characteristics of wall turbulence with a passive scalar, *Journal of Fluid Mechanics*. **196**, 157-185, 1988.

[25] A.F. Orlando, R.J. Moffat, and W.M. Kays Turbulent transport of heat and momentum in a boundary layer subject to deceleration, suction and variable wall temperature, Report HMT-17, Thermoscience Division, Stanford University, 1974.

[26] H.D. Pasinato, and K. Squires. On the Effect of Perturbed Channel FLow on Thermal Field, *ENIEF2006*, Santa Fe, 2006.

[27] P.R. Spalart and M.K. Strelets. Mechanisms of transition and heat transfer in a separation bubble, *Journal of Fluid Mechanics*. **403**, 329-349, 2000.

[28] C.S. Subramanian and R.A. Antonia. Effect of Reynolds number on a slightly heated turbulent boundary layer. *Int. J. Heat Mass Transfer*, **24**(11), 1833-1846, 1981.

[29] H. Suzuki, K. Suzuki, and T. Sato. Dissimilarity between heat and mass transfer in a turbulent boundary layer disturbed by a cylinder. *Int. J. Heat Mass Transfer*, **31**, (2), 259-265, 1988.

[30] H. Tenneks and J.L. Lumnly. A First Course in Turbulence. *The MIT Press*, Cambridge, Massachusetts, 1972.

[31] Z. Zaric. Wall turbulence structure and convection heat transfer. *Int. J. Heat and Mass Transfer*, **18**, 831-842, 1975.